Novel SIRT1 inhibitor 15-deoxy-$\Delta^{12,14}$-prostaglandin J_2 and its derivatives exhibit anticancer activity through apoptotic or autophagic cell death pathways in SKOV3 cells

IN HWAN TAE[1], EUN YOUNG PARK[2], PRASANTA DEY[1], JI YEON SON[1], SEOK-YONG LEE[1], JEE H. JUNG[2], SALONI SALONI[3], MI-HYUN KIM[3] and HYUNG SIK KIM[1]

[1]School of Pharmacy, Sungkyunkwan University, Suwon, Gyeonggi 16419; [2]College of Pharmacy, Pusan National University, Busan 46241; [3]College of Pharmacy, Gachon University, Incheon 21936, Republic of Korea

Received January 30, 2018; Accepted August 13, 2018

DOI: 10.3892/ijo.2018.4561

Abstract. Clinically relevant sirtuin (SIRT) inhibitors may possess antitumor activities. A previous study indicated that 15-deoxy-$\Delta^{12,14}$-prostaglandin J_2 (15d-PGJ_2) exhibited potent anticancer activity by SIRT1 inhibition. Therefore, the aim of the present study was to investigate whether its derivatives (J11-C1 and J19) exhibited anticancer activity against ovarian cancer SKOV3 cells. Cell viability was determined using an MTT assay. Cell cycle arrest, apoptosis and autophagy were determined using flow cytometry or western blot analysis. J11-Cl and J19 were less cytotoxic to SKOV3 cells compared with 15d-PGJ_2. Molecular docking studies supported the interactions of 15d-PGJ_2, J11-Cl and J19 with various amino acids in SIRT1 proteins. Similar to 15d-PGJ_2, J11-C1 and J19 inhibited SIRT1 enzymatic activity and decreased SIRT1 expression levels in a concentration-dependent manner. J11-C1 induced apoptotic cell death more effectively compared with J19, which was associated with markedly decreased expression of the anti-apoptotic molecule B-cell lymphoma 2 (Bcl-2). Furthermore, the levels of light chain 3-II (LC3-II) and beclin-1 were clearly induced in SKOV3 cells treated with J11-Cl. Thus, 15d-PGJ_2 and its derivatives exhibited anticancer activity possibly by inducing apoptotic or autophagic cell death pathways. Collectively, the results of the present study suggest that 15d-PGJ_2 and its derivatives exerted antitumor activity by selectively modulating the expression of genes associated with cell cycle arrest, apoptosis and autophagy. Notably, J11-C1 is a novel candidate SIRT1 inhibitor with anticancer activity.

Correspondence to: Professor Hyung Sik Kim, School of Pharmacy, Sungkyunkwan University, 2066 Seobu, Suwon, Gyeonggi 16419, Republic of Korea
E-mail: hkims@skku.edu

Key words: 15-deoxy-$\Delta^{12,14}$-prostaglandin J_2, J11-Cl, sirtuin 1, apoptosis, autophagy, ovarian cancer

Introduction

Sirtuins (SIRTs) are class III histone deacetylases (HDACs) that have been identified to serve important biological functions, including aging, energy mobilization and stress responses (1,2). Furthermore, SIRTs are involved in the regulation of cancer cell apoptosis and are potential targets for novel anticancer drugs that regulate the levels of deacetylated histone proteins, p53 and several transcriptional factors (3,4). Several SIRT1 inhibitors, such as Ex527, sirtinol and salermide, exhibit potent anticancer activity in various cancer cell lines (5,6). Previously, we demonstrated that a novel SIRT inhibitor, psammaplin A, increased p53 acetylation and subsequently induced apoptotic death in MCF-7/Adr cells (7). In addition, Chu *et al* (8) demonstrated that patients with chemoresistant tumors overexpressed SIRT1; furthermore, the inhibition of SIRT1 expression decreased multidrug resistance 1 (MDR1) expression and increased drug sensitivity.

15-Deoxy-$\Delta^{12,14}$-prostaglandin J_2 (15d-PGJ_2) was revealed to exhibit pharmacological activities, including anti-inflammatory, anti-fibrotic and apoptotic effects, through peroxisome proliferator-activated receptor γ-independent signaling pathways such as the nuclear factor-κB (NF-κB), signal transducer and activator of transcription 1 (STAT1) and p53-dependent signaling pathways (9,10). Furthermore, 15d-PGJ_2 was identified to induce apoptosis of various cancer cells through caspase-dependent signaling pathways (11). A previous study demonstrated that 15d-PGJ_2 inhibited the migration of A2780/AD cells, possibly via NF-κB inhibition resulting from HDAC1 inhibition. The mechanisms of action underlying these novel effects of 15d-PGJ_2 on SIRT1 and HDAC1 gene expression and enzyme activities were elucidated (12). In the present study, the effects of novel SIRT1 inhibitors (J11-Cl and J19), with a 15d-PGJ_2 scaffold (11,12), on ovarian cancer cells were investigated.

Methyl jasmonate is a member of the jasmonate family of plant stress hormones, the most potent regulator of defense-associated mechanisms in plants (13). On the basis of its structural similarity to that of 15d-PGJ_2, methyl jasmonate (J-11) was investigated for SIRT activity, and its functional mechanisms of regulation of cancer cell death pathways were

investigated. A previous study indicated that an α-haloenone analog, J7, exhibited enhanced *in vitro* anti-inflammatory potency (14,15).

Materials and methods

Reagents. 15d-PGJ$_2$ (87893-55-8) and 3-methyladenine (3-MA; 5142-23-4) were purchased from Cayman Chemical Company (Ann Arbor, MI, USA). J11-Cl and J19 were synthesized in-house. The chemical structures of the drugs are presented in Fig. 1A. Dulbecco's modified Eagle's medium (DMEM), fetal bovine serum (FBS) and cell culture supplements were obtained from Gibco; Thermo Fisher Scientific, Inc. (Waltham, MA, USA). Primary antibodies against SIRT1 (cat. no. 8469; 1:1,000), SIRT2 (cat. no. 12672; 1:1,000), SIRT4 (cat. no. sc-135798; 1:500), SIRT5 (cat. no. 8779; 1:1,000), SIRT6 (cat. no. 8771; 1:1,000), B-cell lymphoma-2 (Bcl-2; cat. no. 15071; 1:500), Bcl-2-associated X protein (Bax; cat. no. 5023; 1:1,000), β-actin (cat. no. 3700; 1:1,000), light chain 3 (LC3; cat. no. 3868; 1:1,000), beclin-1 (cat. no. 4122; 1:1,000), autophagy-related 3 (Atg3; cat. no. 3415; 1:1,000), Atg5 (cat. no. 12994; 1:1,000), Atg7 (cat. no. 8558; 1:1,000), α-tubulin (cat. no. 3873; 1:1,000), cleaved caspase-3 (cat. no. 9661; 1:500), cleaved caspase-9 (cat. no. 7237; 1:1,000), poly(ADP-ribose) polymerase (PARP; cat. no. 9541; 1:1,000) and acetylated p53 (cat. no. 2570; 1:500) were purchased from Cell Signaling Technology (Beverly, MA, USA). Horseradish peroxidase-conjugated secondary antibodies [anti-mouse immunoglobulin G (IgG); cat. no. sc-516102 or anti-rabbit IgG; cat no. sc-2357] were purchased from Santa Cruz Biotechnology, Inc. (Dallas, TX, USA). All other chemicals were purchased from Sigma-Aldrich; Merck KGaA. All drugs were dissolved in dimethyl sulfoxide (DMSO) and stored at -20˚C until use. Chemical agents were diluted to appropriate concentrations with culture medium supplemented with 1% FBS. The final concentration of DMSO was <0.1% (v/v). DMSO was also present in the corresponding controls.

SIRT1 enzyme activity. SIRT1 enzymatic activity was assessed using commercial kits (cat. no. ab156065) from Abcam (Cambridge, UK), according to the manufacturer's protocol. First, assay buffer [50 mM Tris/HCl, pH 8.0, 137 mM NaCl, 2.7 mM KCl, 1 mM $MgCl_2$ and 1 mg/ml bovine serum albumin (BSA)], SIRT1 enzyme, and either the solvent dimethylformamide (DMF) or different concentrations of the drugs (15d-PGJ$_2$, J19 or J11-C1 dissolved in DMF) were mixed with the substrate (p53) and co-substrate (NAD^+) for 45 min. Deacetylation reactions were conducted at 37˚C for 60 min, and stopped by adding 50 µl stop solution containing the developer, followed by incubation at 37˚C for 30 min. Fluorescence intensity was determined by reading fluorescence using a SpectraMax M2 microplate reader (Molecular Devices, LLC, Sunnyvale, CA, USA) with an excitation wavelength of 350 nm and an emission wavelength of 450 nm. Calculations of net fluorescence were made after subtracting values for a blank consisting of buffer without NAD.

Docking simulations of sirtinol, 15d-PGJ$_2$, J11-Cl and J19 ligand and target structure. The X-ray crystal structure of SIRT1 was selected from the Research Collaboratory for Structural Bioinformatics Protein Data Bank (PDB; code 4I5I) and prepared using the protein preparation wizard available in the Glide tool in Maestro (version 10.2; Schrödinger, LLC, New York, NY, USA). During the process, the missing side and back chains were included (16). The protein preparation wizard facility has two components: Preparation and refinement. Following ensuring the chemical accuracy, the preparation component adds hydrogen and neutralizes a side chain that is neither close to the binding cavity nor involved in the formation of salt bridges. The all-atom-optimized potentials for liquid simulations (OPLS-AA) force field was used for this purpose, and then the active site of protein was defined. Glide uses the full OPLS-AA force field at an intermediate docking stage and is considered to be more sensitive to geometrical detail compared with other docking algorithms. The water molecule occupying the protein structure was not suitable for the docking study, therefore it was removed. Finally, the optimization and minimization processes were performed until the average root mean square deviation of the non-hydrogen atoms reached 0.3 Å (17). This was followed by the generation of energy grids using the Glide protocol, as previously described (18-20). The docked ligand was used to define the energy grid boundaries with the default options. These grids were used to score the ligand 'in place' with the XP scoring function. It should be noted that considering the computational protocol followed for the generation of the covalent complexes, the XP Glide Score values can be used only in a qualitative sense to determine the binding of various ligands. The Glide XP scoring functions include improvements to the scoring of hydrogen bonds, the detection of buried polar groups, and the detection of π-cation and π-π stacking interactions. The result of the docking calculation is a top-scored predicted complex that is evaluated using the scoring function. The compounds sirtinol, 15d-PGJ$_2$, J11-Cl and J19 were prepared using the LigPrep software (version 3.4; Schrödinger, LLC), which can generate a number of structures from each input structure with various ionization states, tautomers, stereochemistries and ring conformations. This process eliminates molecules using various criteria including the molecular mass, specified numbers and types of functional groups present with correct chiralities for each successfully processed input structure. The OPLS 2005 force field was used for the optimization, which produced the low-energy isomer of the ligand (21). Finally, all ligand molecules formed in the complex structure for input were docked.

Cell culture. Human ovarian cancer cell lines (SKOV3 and OVCAR3) and normal kidney epithelial cell lines (HK-2 and NRK-52E were purchased from the American Type Culture Collection (ATCC; Manassas, VA, USA). SKOV3, OVCAR3, or NRK-52E cells were maintained in DMEM supplemented with 10% FBS, 4 mmol L-glutamine, 100 U/ml penicillin and 100 µg/ml streptomycin (Gibco; Thermo Fisher Scientific, Inc.). HK-2 cells were maintained in DMEM/Ham's F12 (Gibco; Thermo Fisher Scientific, Inc.) supplemented with 5 µg/ml insulin (Gibco; Thermo Fisher Scientific, Inc.), 5 µg/ml transferrin (Gibco; Thermo Fisher Scientific, Inc.), 100 U/ml penicillin, 100 g/ml streptomycin, 0.1 µmol/l hydrocortisone, 2 nmol/l L-glutamine plus 10% FBS. The cell

cultures were incubated at 37˚C in a humidified atmosphere containing 5% CO_2.

Cytotoxicity assay. Cell viability was determined using MTT (5 mg/ml; Sigma-Aldrich; Thermo Fisher Scientific, Inc.). The cells were seeded in 96-well plates at a density of $2x10^3$ cells/well. Following incubation at 37˚C for 24 h, the cells were treated with 15d-PGJ_2 (0.05-20 μM), J11-C1 (1-160 μM) or J19 (1-160 μM) and cultured for a further 24, 48 or 72 h. Following incubation, 15 μl MTT reagent was added to each well and plates were incubated at 37˚C for 3 h in the dark. The supernatant was aspirated and formazan crystals were dissolved in 150 μl DMSO at 37˚C for 15 min with gentle agitation. The absorbance of each well was measured at 540 nm using a VersaMax microplate reader (Molecular Devices LLC, Sunnyvale, CA, USA). Three independent experiments were performed for each condition and normalized to the absorbance of wells containing medium only (0%) or untreated cells (100%). The half-maximal inhibitory concentration (IC_{50}) values were calculated from the sigmoidal concentration-response curves using SigmaPlot (version 12; Systat Software, Inc., San Jose, CA, USA).

Cell cycle analysis. Cells were treated with 15d-PGJ_2 (1, 5 or 10 μM), J11-Cl (1, 5 or 25 μM), or J19 (1, 5 or 25 μM) for 48 h or vincristine sulfate (BML-T117-0005; Enzo Life Sciences, Inc., Farmingdale, NY, USA) at 5 nM as a positive control. The total number of cells, including those in suspension and those adhered to the walls of the wells, were harvested separately to identify sub-G_1 or other cell cycle stages, and were washed in 1% BSA before fixing in 95% ice-cold ethanol containing 0.5% Tween-20 for 1 h at -20˚C. The cells ($1x10^6$) were washed in a solution containing 1% BSA, stained with ice-cold propidium iodide (PI) solution (10 μg/ml PI and 100 μg/ml RNase in PBS) and incubated in the dark for 30 min at room temperature. The data were acquired and analyzed using a flow cytometer (BD Biosciences, San Jose, CA, USA).

Detection of apoptosis using Annexin V/PI staining. Cells were seeded in 6-well plates (Labtek; Nalge Nunc International, Penfield, NY, USA) at $1x10^5$ cells/well and allowed to attach overnight. After 24 h of incubation at 37˚C, the cells were washed with serum-free medium and treated with different concentrations of the drugs in 200 μl medium/well for 48 h. Following induction of apoptosis, the supernatant was collected and the adherent cells ($2x10^6$ cells) were trypsinized from the plates. The collected cells were washed twice with PBS and centrifuged at 600 x g for 5 min. Each pellet was resuspended in 50 μl 4-(2-hydroxyethyl)-1-piperzaine-ethanesulfonic acid (HEPES) buffer (10 mM HEPES, 135 mM NaCl and 5 mM $CaCl_2$). Cells ($2x10^6$ cells in 100 μl buffer) were transferred to flow cytometry tubes and 2 μl each of Annexin V-fluorescein isothiocyanate (FITC) and PI (each at 1 mg/ml) were added. Following incubation for 5 min at room temperature in the dark, 400 μl binding buffer was added to each tube. Samples were analyzed using a flow cytometer (Guava® easyCyte flow cytometer, EMD Millipore, Billerica, MA, USA).

Western blot analysis. SKOV3 cells were cultured in DMEM at 37˚C in a humidified atmosphere containing 5% CO_2. Following incubation for 24 h, the cells were treated with 15d-PGJ_2 (1, 5 or 10 μM), J11-Cl (1, 5 or 25 μM) or J19 (1, 5 or 25 μM), cultured for 48 h, harvested using trypsin digestion, and then washed twice with ice-cold PBS. To isolate total proteins, the cells were first suspended in PRO-PREP™ protein extraction solution (Intron Biotechnology, Inc., Seongnam, Korea). Protein concentrations were determined using a Bicinchoninic Acid protein assay kit (Bio-Rad Laboratories, Inc., Hercules, CA, USA), according to the manufacturer's protocol. Protein samples (20 μg) of the cell extracts were separated by SDS-PAGE (6-15% gels) and transferred onto a polyvinylidene difluoride membrane (EMD Millipore), which was incubated for 1 h in TNA buffer (25 mM Tris/HCl, pH 8.5, 192 mM glycine and 20% methanol) and blocked with 5% skimmed milk powder in PBS. Subsequently, the membrane was incubated with various primary antibodies against SIRTs, Bax, Bcl-2, β-actin, PARP, cleaved caspase-3, cleaved caspase-9, p53, acetylated p53, LC3, beclin-1, Atg3, Atg5 and Atg7 at 4˚C overnight. Following washing for 1 h with TNA buffer, the membrane was incubated with horseradish peroxidase-conjugated anti-mouse or anti-rabbit secondary antibodies (1:10,000) for 1 h at room temperature. The blots were developed using an Enhanced Chemiluminescence Plus kit (GE Healthcare Life Sciences, Little Chalfont, UK). The data were acquired and analyzed using an ImageSaver6 (ATTO Corp., Tokyo, Japan).

Reverse transcription-polymerase chain reaction (RT-PCR). Total RNA was isolated using TRIzol® reagent (Gibco; Thermo Fisher Scientific, Inc.) according to the manufacturer's protocol. Samples of 2 μg RNA were reverse-transcribed for 50 min at 42˚C in a 20 μl reaction mixture containing 1 μl oligonucleotide $(dT)_{15}$ primer (0.5 μg), 10 mM dNTP mixture, 25 mM $MgCl_2$ (4 μl), 0.1 M dithiothreitol (2 μl), RNaseOUT inhibitor (1 μl; Invitrogen; Thermo Fisher Scientific, Inc.), Superscript II (50 units) and X10 reverse transcription buffer (2 μl), followed by denaturation at 68˚C for 15 min. The cDNAs obtained were further amplified using PCR with the specific primers. The primers sets and PCR conditions are presented in Table I. The number of PCR cycles was estimated in a preliminary study and optimized in the exponential phase of PCR. The PCR products were subjected to electrophoresis on 2% agarose gels and visualized by ethidium bromide staining and UV transillumination (WSE-5600 CyanoView; ATTO Corp.). The molecular sizes of the amplified products were determined by comparison with a molecular mass marker (100 bp DNA ladder; Intron Biotechnology, Inc.) that was run in parallel with the RT-PCR products. Each assay was performed three times.

Acridine orange staining. SKOV3 cells were seeded in T-25 flasks and treated with 15d-PGJ_2 (1, 5 or 10 μM), J11-Cl (1, 5 or 25 μM) or J19 (1, 5 or 25 μM) for 48 h when the cells reached 70% confluence. At the appropriate time points, the cells were treated with 1 μg/ml acridine orange (2.7 μM) in serum-free medium at 37˚C for 15 min at room temperature. Following washing with PBS, the formation of acidic vesicular organelles (AVOs) was observed using fluorescence microscopy (FV10i; Olympus Corp., Tokyo, Japan). The cytoplasm and nuclei of the stained cells fluoresced bright green, whereas the acidic AVOs

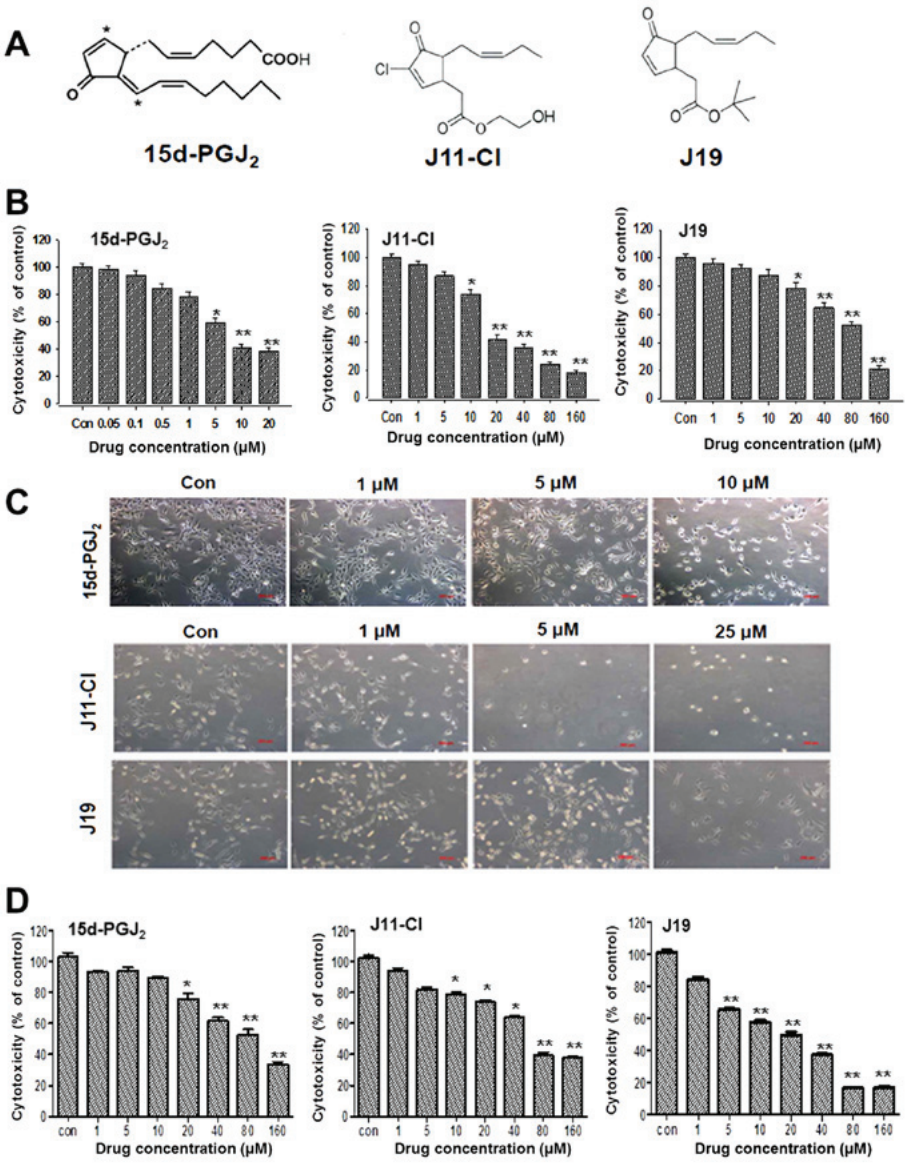

Figure 1. Assessment of the cytotoxicity of the compounds in SKOV3 and OVCAR3 cells. (A) Chemical structures of 15d-PGJ$_2$, J11-Cl and J19. (B) SKOV3 cells were treated with 15d-PGJ$_2$, J11-Cl or J19 at various concentrations for 48 h, and cell viability was determined using an MTT assay. (C) The morphological changes of SKOV3 cells following treatment with 15d-PGJ$_2$, J11-Cl or J19 for 48 h. Magnification, x100. (D) OVCAR3 cells were treated with 15d-PGJ$_2$, J11-Cl or J19 at various concentrations for 48 h. Cell viability was determined using an MTT assay. Results are presented as the mean ± standard error of the mean of three independent experiments. *P<0.05, **P<0.01 vs. control. 15d-PGJ$_2$, 15-deoxy-$\Delta^{12,14}$-prostaglandin J$_2$.

fluoresced bright red. Additionally, green (510-530 nm) and red (650 nm) fluorescence emission from 1x10^4 cells exposed to blue (488 nm) excitation light was determined using a flow cytometer.

Monodansylcadaverine (MDC) incorporation assay. Autophagic vacuoles were also detected by incubation with 50 μmol/l MDC in PBS at 37˚C for 10 min. Following incubation, the cells were washed four times with ice-cold PBS and were fixed with 3.75% paraformaldehyde in PBS. The cells were immediately analyzed using a confocal microscope (FV10i) equipped with a filter system (excitation wavelength, 380 nm; emission filter, 525 nm).

Statistical analysis. Statistical analyses were carried out using GraphPad Prism software (version 5.03; GraphPad Software, Inc., La Jolla, CA, USA). All numerical data are presented as the mean ± standard error of the mean. Statistical analyses were performed using Student's t-test or Mann-Whitney U test. One-way analysis of variance with Tukey's post hoc test to assess differences among specific groups was used for comparison among multiple values. P<0.05 was considered to indicate a statistically significant difference.

Results

Effects of 15d-PGJ$_2$, J19 and J11-C1 on the viability of ovarian cancer cells. Different cancer cell lines were used to screen the *in vitro* cytotoxic activity of 15d-PGJ$_2$ and its derivatives. Cell viability was determined using an MTT assay. Human ovarian cancer SKOV3 cells were treated with the indicated concentrations of agents for 48 h. 15d-PGJ$_2$ significantly decreased cell

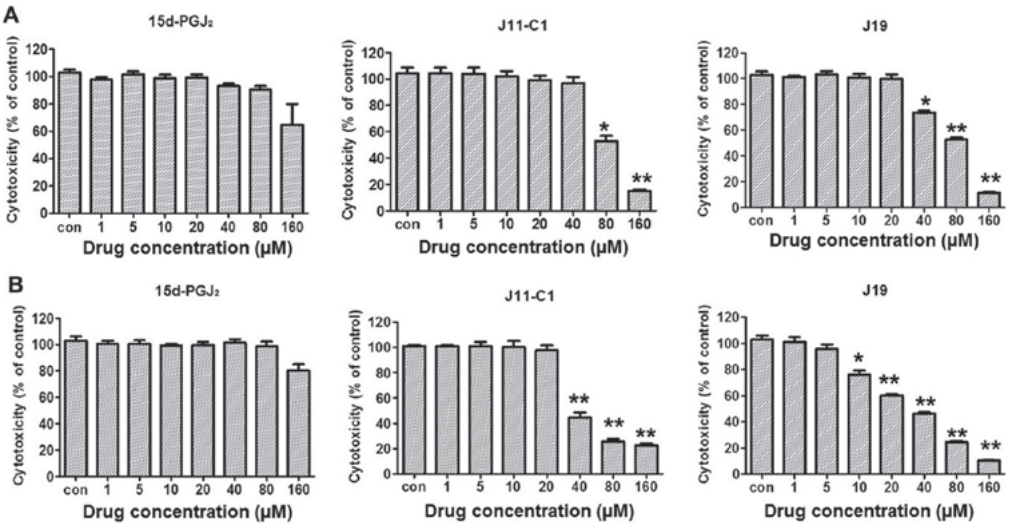

Figure 2. Cytotoxicity of compounds against normal cells. (A) Normal kidney tubular epithelial HK-2 cells and (B) normal rat kidney NRK-52E cells were treated with 15d-PGJ_2, J11-Cl or J19 at various concentrations for 48 h. Cell viability was determined using an MTT assay. Results are presented as the mean ± standard error of the mean of three independent experiments. $^{*}P<0.05$, $^{**}P<0.01$ vs. control. 15d-PGJ_2, 15-deoxy-$\Delta^{12,14}$-prostaglandin J_2.

Table I. Primer sequences for the polymerase chain reaction.

Gene name	Primer sequence	Product length (bp)	T_m (˚C)	Cycling conditions
SIRT1	F: 5'-GACTCCAAGGCCACGGATAG-3' R: 5'-GTGGAGGTATTGTTTCCGGC-3'	110	59.89 58.91	95˚C for 5 min; 34 cycles of 95˚C for 15 sec, annealing at 57˚C for 15 sec and 72˚C for 15 sec; 72˚C for 10 min
SIRT2	F: 5'-GGCAGTTCAAGCCAACCATC-3' R: 5'-CCACCAAGTCCTCCTGTTCC-3'	132	59.76 59.96	95˚C for 5 min; 35 cycles of 95˚C for 15 sec, annealing at 57˚C for 15 sec and 72˚C for 15 sec; 72˚C for 10 min
SIRT4	F: 5'-AGGGTCCTGTGCTTGGATTG-3' R: 5'-GGTTTCAGATGGCCTCCACA-3'	172	59.96 59.96	95˚C for 5 min; 32 cycles of 95˚C for 15 sec, annealing at 57˚C for 15 sec and 72˚C for 15 sec; 72˚C for 10 min
GAPDH	F: 5'-GAGTCAACGGATTTGGTCGT-3' R: 5'-TGTGGTCATGAGTCCTTCCA-3'	512	58.21 58.27	95˚C for 5 min; 32 cycles of 95˚C for 15 sec, annealing at 56˚C for 15 sec and 72˚C for 15 sec; 72˚C for 10 min

SIRT, Sirtuin; F, forward; R, reverse.

viability in a concentration-dependent manner with an IC_{50} of 7.58 μM after 48 h of treatment. Similarly, J11-C1 and J19 markedly affected SKOV3 cell viability in a concentration-dependent manner, but the IC_{50} values of J11-C1 (17.6 μM) and J19 (83 μM) were much higher compared with that of 15d-PGJ_2 (Fig. 1B). During incubation with 15d-PGJ_2, the cell morphology was altered to an enlarged and elongated form. However, SKOV3 cells also appeared to be more stretched following J11-Cl treatment, with a different cell morphology phenotype from that of the control cells. Following treatment with J19, the cells were initially rounded and shrunken with larger cytoplasm and distinct cellular boundaries (Fig. 1C). The cytotoxicity of 15d-PGJ_2 and its derivatives against the other ovarian cancer cell line used, OVCAR3 cells, were compared. The results indicated that the cytotoxic effect of 15d-PGJ_2, (IC_{50}, 80.7 μM), J11-Cl (49.2 μM) or J19 (20.3 μM) was lower compared with that in SKOV3 cells (Fig. 1D), therefore, SKOV3 cells were selected for our subsequent experiments. The cytotoxic effect of 15d-PGJ_2 and its derivatives against normal cells was examined using an MTT assay. Normal kidney proximal tubule epithelial HK-2 or NRK-52E cells were treated with 15d-PGJ_2 or its derivatives for 48 h. No significant cytotoxicity was observed in HK-2 or NRK-52E cells at 80 μM 15d-PGJ_2 (Fig. 2A), which significantly affected SKOV3 cells, suggesting that the cytotoxic effect of the 15d-PGJ_2 was selective towards cancer cells.

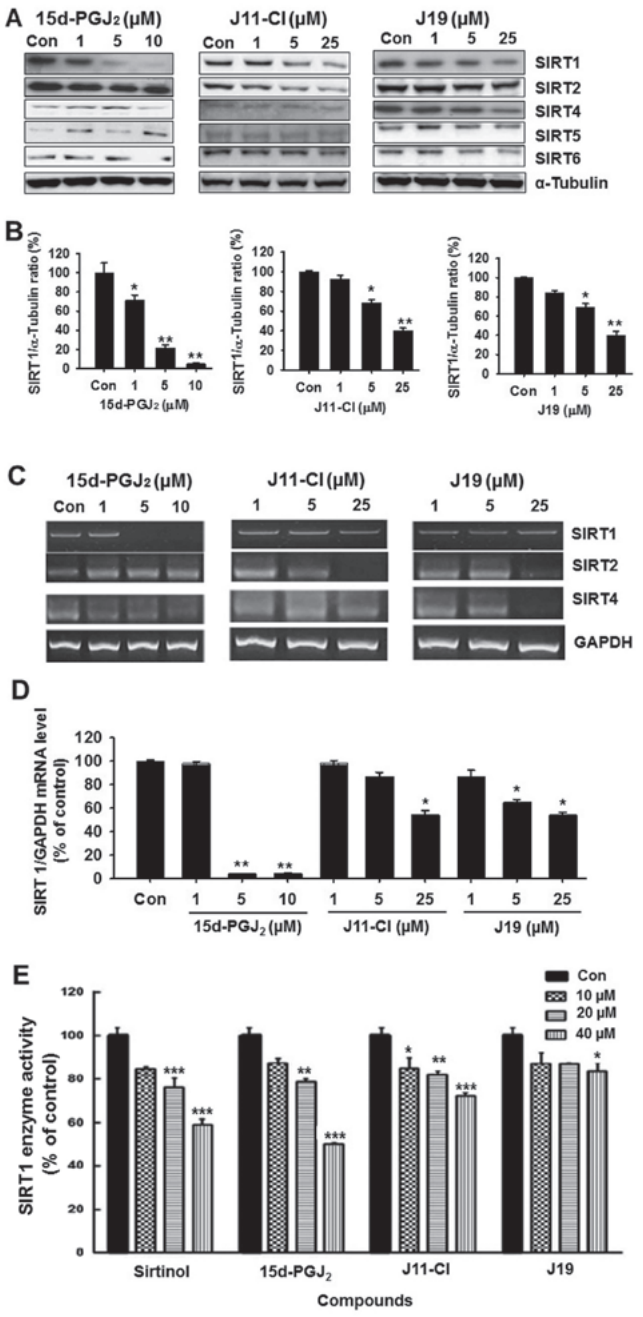

Figure 3. Effects of 15d-PGJ$_2$, J11-Cl and J19 on SIRT expression and SIRT1 enzyme activity. (A) SKOV3 cells were treated with various concentrations of 15d-PGJ$_2$, J11-Cl and J19 for 48 h. The proteins were isolated and western blotting analysis was performed with antibodies against SIRT1, SIRT2, SIRT4, SIRT5 and SIRT6. Western blot images are representative of SKOV3 cells from triplicate experiments. (B) Protein band quantification using densitometry from three independent experiments. (C) mRNA expression of SIRT1, SIRT2 and SIRT4 in SKOV3 cells treated with 15d-PGJ$_2$, J11-Cl and J19. (D) Quantification of mRNA levels from three independent experiments using densitometry. (E) Effects of sirtinol, 15d-PGJ$_2$, J11-Cl and J19 on total SIRT1 enzymatic activity using a commercial kit. Results are presented as the mean ± standard error of the mean of three independent experiments. *P<0.05, **P<0.01, ***P<0.001 vs. control. 15d-PGJ$_2$, 15-deoxy-$\Delta^{12,14}$-prostaglandin J$_2$; SIRT, sirtuin; Con, control.

SIRT enzymatic activity and expression in SKOV3 cells. The effect of 15d-PGJ$_2$ and its derivatives on SIRT protein expression was examined in SKOV3 cells using western blotting with specific antibodies against acetylated SIRT1, SIRT2, SIRT4, SIRT5 and SIRT6. As presented in Fig. 3A, 15d-PGJ$_2$ markedly decreased the expression of SIRT1, at 1 μM. However, a high concentration (5 μM) of J11-Cl and J19 markedly decreased SIRT1 protein levels (Fig. 3A and B). To confirm the expression of SIRTs in SKOV3 cells, the mRNA levels of SIRT1, SIRT2 and SIRT4 in SKOV3 cells treated with 15d-PGJ2 (1, 5 or 10 μM), J11-Cl (1, 5 or 25 μM), or J19 (1, 5 or 25 μM). As presented in Fig. 3C and D, mRNA levels of SIRT1 and SIRT4 were significantly decreased following 15d-PGJ$_2$ treatment (5 and 10 μM). In addition, the mRNA levels of SIRT2 were markedly decreased in SKOV3 cells by 25 μM J11-Cl and J19 treatment (Fig. 3C). The effects of 15d-PGJ$_2$, J19 and J11-C1 on total SIRT1 enzymatic activity were investigated. Sirtinol was used as a reference compound for SIRT1 inhibitor. As presented in Fig. 3E, sirtinol significantly inhibited SIRT1 enzyme activity in a concentration-dependent manner. It was identified that 15d-PGJ$_2$ and J11-Cl significantly decreased SIRT1 enzymatic activity at high concentrations. Similar to the protein levels, J19 only significantly inhibited SIRT1 enzyme activity at high concentrations (Fig. 3E).

Molecular docking analysis. The aims of the molecular docking study were to elucidate whether 15d-PGJ$_2$, J11-Cl or J19 modulate anticancer targets and identify the actual binding pocket against the molecular target of SIRT1. The orientations and binding affinities of the drugs to SIRT1 (PDB code 4I5I) were identified. The docking results for sirtinol revealed a high docking score of -9.41 to -8.27 and the formation of a hydrogen bond of 1.94 Å (-C=O) to the backbone of Gln^{345} and π-π stacking bond lengths of 4.7 and 5.2Å with Phe^{273} and Phe^{414}. In the docking pose, the chemical natures of the binding site residues within a radius of 3 Å from the bound compound are presented in Fig. 4A. Similarly, the docking results of 15d-PGJ$_2$ revealed a docking score of -9.43 to -6.82 and formed three hydrogen bonds of 2.37 (O=C-NH-), 2.09 (-C=O) and 1.77 Å (O=C-NH-) to Asp^{348} and Ile^{347} (Fig. 4B). Likewise, the docking results of J11-C1 revealed a docking score of -7.34 to -3.98 and formed two hydrogen bonds with lengths of 1.98 Å (-C=O) to PRo$_{271}$ and of 2.51 Å (O=C-NH-) to Ile$_{347}$ (Fig. 4C). Lastly, the docking results of J19 revealed a low docking score of -4.33 to -2.85 and formed two hydrogen bonds with lengths of 2.18 and 2.24 Å (-NH=C-NH2) to Arg^{274} (Fig. 4D). In the docking pose, the binding site residues were His^{363}, Ile^{411}, Ala^{262}, Phe^{413}, Phe^{273}, Phe^{414}, Phe^{297}, Phe^{297} and Asn^{346}; thus, the bound drugs exhibited good binding affinity and marked hydrophobic interactions, which may lead to greater stability and activity. The overall interaction of the binding site pocket (within a radius of 3 Å) is summarized in Table II.

Effects of 15d-PGJ$_2$, J19 and J11-C1 on cell cycle progression in SKOV3 cells. SIRT inhibitors exhibited moderate cytotoxicity towards various human cancer cells through the induction of cell cycle arrest at a specific phase. The effects of 15d-PGJ$_2$ and its derivatives on cell cycle progression were determined using flow cytometry, and 15d-PGJ$_2$ was identified to significantly increase the number of cells in G$_2$/M phase after 48 h of incubation (Fig. 5). Similarly, J11-C1 and J19 significantly increased the population of SKOV3 cells in G$_2$/M

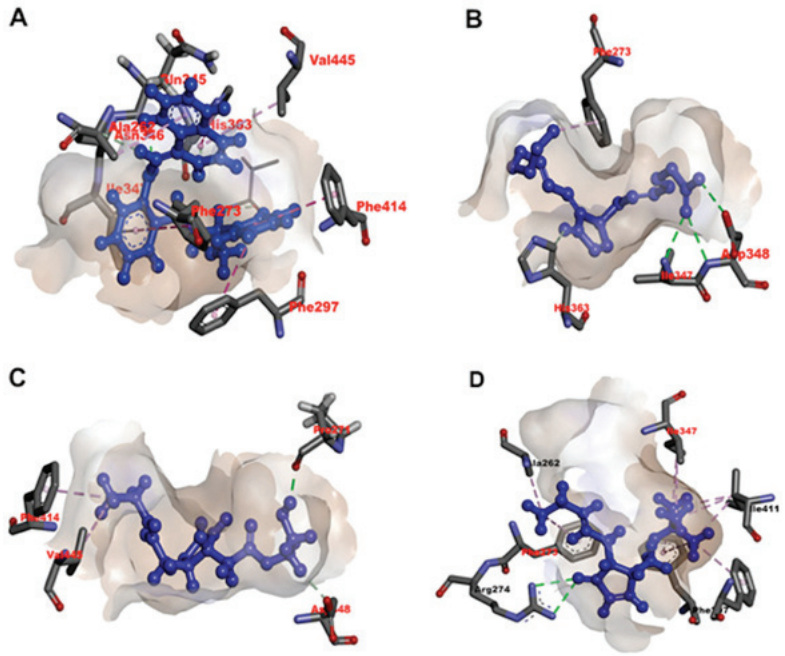

Figure 4. Identification of sirtinol-, 15d-PGJ_2-, J11-Cl- and J19-binding sites on SIRT1 using molecular docking simulations. Effective non-covalent interactions between the residues of SIRT1 and ligands (A) sirtinol, (B) 15d-PGJ_2, (C) J11-Cl and (D) J19 are depicted with dashed lines. Green, magenta and pink indicate hydrogen bond, π-π stacking and hydrophobic interaction, respectively. A black dashed line in a ligand indicates resonance in its functional group. 15d-JG_2, 15d-PGJ_2, 15-deoxy-$\Delta^{12,14}$-prostaglandin J_2.

Table II. Identification of inhibitor-binding site in human SIRT1 using molecular docking and dynamics simulations.

Ligand	Docking score (mean ± standard error of the mean)	Amino acids in the binding site within 3.0 Å of ligand	Length of hydrogen bond, Å	No. of hydrogen bonds
Sirtinol	-8.79±0.52	Tyr^{280}, Phe^{414}, Phe^{413}, Val^{412}, Ile^{411}, Phe^{297}, His^{363}, Ile^{316}, Phe^{273}, Arg^{274}, Ile^{347}, Asn^{346}, **Gln^{345}**, Ala^{262}, Gly^{261}, Ser^{441}, Ser^{442}	1.94	1
15d-PGJ_2	-8.10±1.28	Ala^{262}, Ser^{265}, **Asp^{348} (a_1, a_2)**, **Ile^{347} (b)**, Asn^{346}, Ile^{270}, Phe^{273}, Arg^{274}, Val^{445}, Tyr^{280}, Ile^{411}, Phe^{413}, Phe^{414}, Phe^{297}, Ile^{316}, His^{363}	a_1, 1.77; a_2, 2.37; b, 2.09 a, 2.51; b, 1.98	3 2
J11-C1	-5.66±1.68	Phe^{297}, Ile^{316}, Ile^{411}, Val^{412}, Phe^{413}, Phe^{414}, His^{363}, Gln^{345}, Asn^{346}, **Ile^{347} (a)**, Asp^{348}, Ser^{265}, Ala^{262}, Ile^{270}, **Pro^{271} (b)**, Asp^{272}, Phe^{273}		
J19	-3.59±0.74	Val^{445}, Tyr^{280}, Phe^{297}, Phe^{414}, Phe^{413}, Val^{412}, Ile^{411}, Ile^{247}, His^{363}, Asn^{246}, Gln^{345}, Gly^{261}, Ala^{262}, **Arg^{274} (a_1, a_2)**, Phe^{273}	a_1, 2.18; a_2, 2.24	2

Hydrogen-bonding residues are in bold. SIRT, sirtuin; 15d-PGJ_2, 15-deoxy-$\Delta^{12,14}$-prostaglandin J_2.

phase following treatment for 48 h. Furthermore, the proportion of cells in G_1 phase was decreased following treatment of SKOV3 cells with the drugs (Fig. 5).

Effects of 15d-PGJ_2, J19 and J11-C1 on apoptotic death of SKOV3 cells. To evaluate the apoptotic death of SKOV3 cells following treatment with 15d-PGJ_2, J19 or J11-C1,

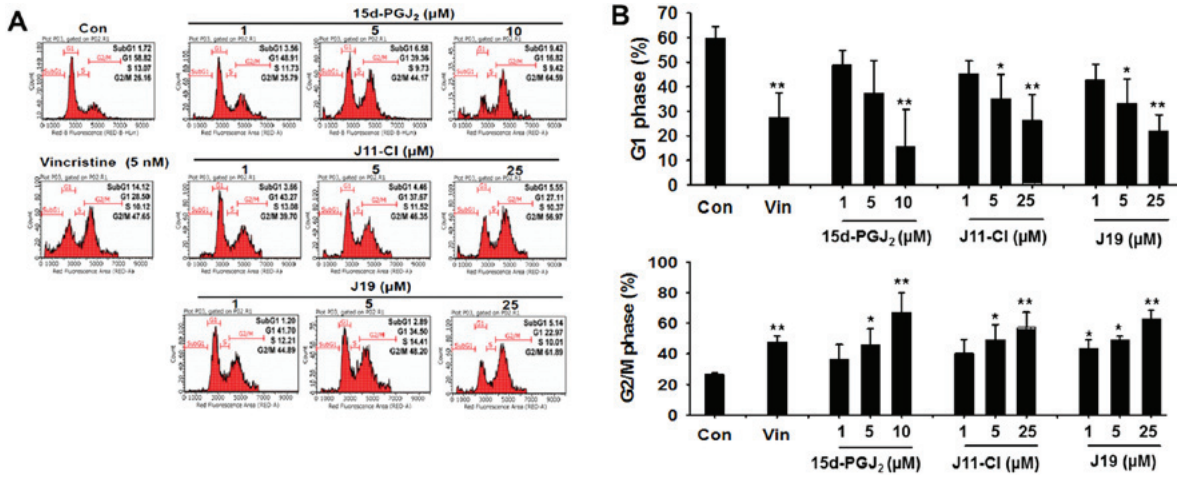

Figure 5. Cell cycle distribution of SKOV3 cells treated with 15d-PGJ$_2$, J11-Cl and J19 at the indicated concentrations for 48 h. (A) Cells were stained with propidium iodide and subjected to flow cytometry to determine the distribution of cells at each phase of the cell cycle, and were compared with untreated cells. Results are representative of three independent experiments. (B) Quantification of cell cycle distribution results, presented as the mean ± standard error of the mean of three independent experiments. *P<0.05, **P<0.01 vs. control. 15d-PGJ$_2$, 15-deoxy-$\Delta^{12,14}$-prostaglandin J$_2$; Con, control; Vin, vincristine.

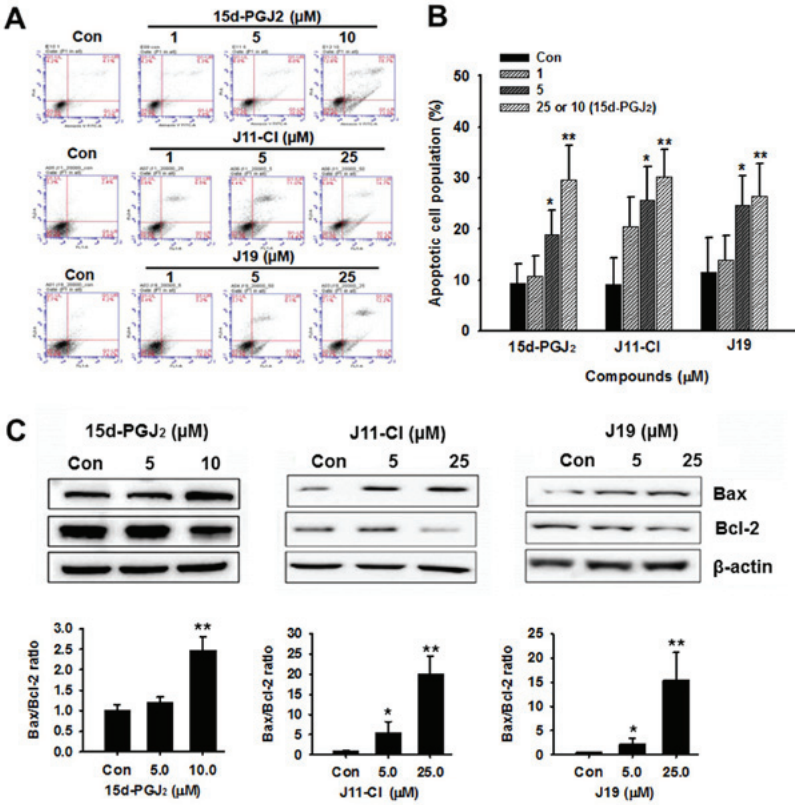

Figure 6. Effects of 15d-PGJ$_2$, J11-Cl and J19 on apoptotic pathways in SKOV3 cells. (A) SKOV3 cells were treated with 15d-PGJ$_2$, J11-Cl or J19 at the indicated concentrations for 48 h. The early and late stages of apoptosis were detected on the basis of Annexin V and propidium iodide staining using flow cytometry. (B) Quantification of apoptosis results, presented as the mean ± standard error of the mean of three independent experiments. (C) Effects of 15d-PGJ$_2$, J11-Cl and J19 on expression of apoptosis-associated proteins in SKOV3 cells. Changes in Bcl-2 and Bax expression were determined using western blotting and quantified from three independent experiments using densitometry.

Annexin V-FITC and PI staining, and western blot analyses were performed. Concentration-dependent increases in apoptotic cell death were observed following treatment with 15d-PGJ$_2$ and its derivatives (Fig. 6A and B). A significant increase in Bax expression and a parallel decrease in Bcl-2 expression were also observed following treatment with these drugs (Fig 6C). In addition, the expression levels of cleaved caspase-3 and -9, cleaved PARP and acetylated p53 were markedly increased in SKOV3 cells following treatment with high concentration of 15d-PGJ$_2$ and its derivatives (Fig. 6D and E).

Effects of 15d-PGJ$_2$, J19 and J11-C1 on autophagic cell death. To evaluate autophagic cell death induced by 15d-PGJ$_2$, J19 and J11-C1, western blot analysis and acridine orange

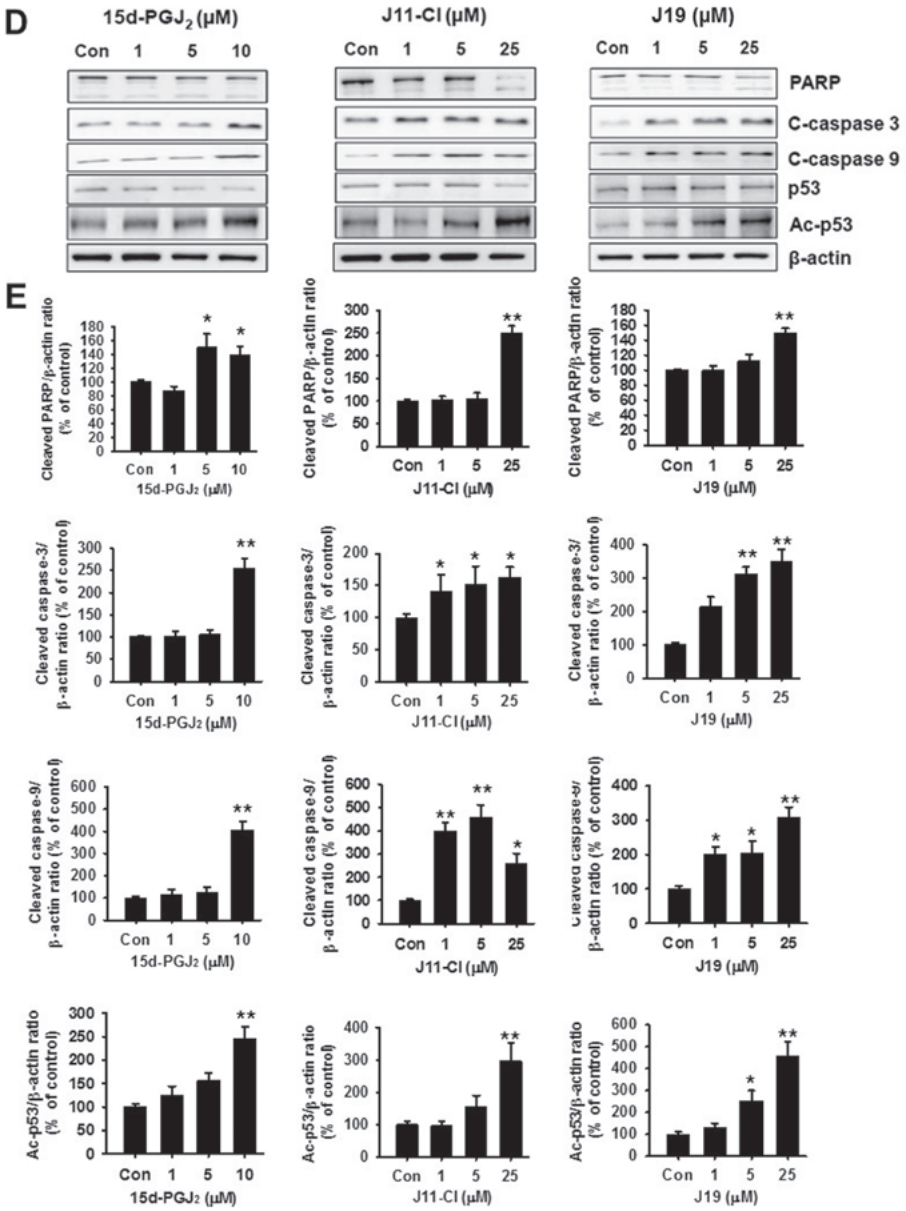

Figure 6. Continued. (D) Effects of 15d-PGJ_2, J11-Cl and J19 on the expression of apoptosis-associated proteins in SKOV3 cells. Changes in PARP, cleaved caspase-3, cleaved caspase-9, p53 and acetylated p53 expression levels were determined relative to expression of β-actin. (E) Quantification of western blot analysis from three independent experiments using densitometry. *P<0.05, **P<0.01 vs. control. 15d-PGJ_2, 15-deoxy-Δ12,14-prostaglandin J_2; Con, control; PARP, poly(ADP-ribose) polymerase; Ac, acetylated; C-, cleaved; Bcl-2, B-cell lymphoma 2.

staining were performed. The conversion of the soluble form of LC3-I into the autophagic vesicle-associated form LC3-II is considered to indicate autophagosome formation (22). As presented in Fig. 7A and B, a high concentration of 15d-PGJ_2, J11-Cl and J19 significantly increased the level of LC3-II, whereas unconjugated LC3-I levels were decreased. Similar to LC3-II, beclin-1 levels increased following treatment with 15d-PGJ_2, J11-Cl or J19 in a concentration-dependent manner (Fig. 7A and B). Subsequently, the induction of autophagy was confirmed by acridine orange staining. Acridine orange is a lysotropic dye that accumulates in acidic organelles in a pH-dependent manner (23-26). At neutral pH, acridine orange emits a green fluorescence, but emits bright red fluorescence within acidic vesicles when protonated and becomes trapped within the organelle (2). As presented in Fig. 7C and D, the control cells exhibited primarily green fluorescence and minimal red fluorescence, which indicated a lack of acidic vesicular organelles. However, drug-treated cells exhibited a more marked red fluorescence 48 h post-treatment compared with the control cells. The increased red fluorescence intensity observed in cultured SKOV3 cells following drug treatment indicated enhanced acidification of vesicular organelles (Fig. 7C). Fig. 7D presents the mean fluorescence intensity of the control and drug-treated cells.

Autophagy inhibition ameliorates cytotoxicity of SKOV3 cells. To investigate the anticancer mechanism of 15d-PGJ_2, J19 or J11-C1 against autophagic cell death in SKOV3 cells, 3-MA (1 mM), an autophagy-specific inhibitor, was incubated with SKOV3 cells. This agent blocks autophagy by inhibiting phosphoinositide 3-kinase, an enzyme required for autophagy (25). As presented in Fig. 8A, the morphological changes indicated

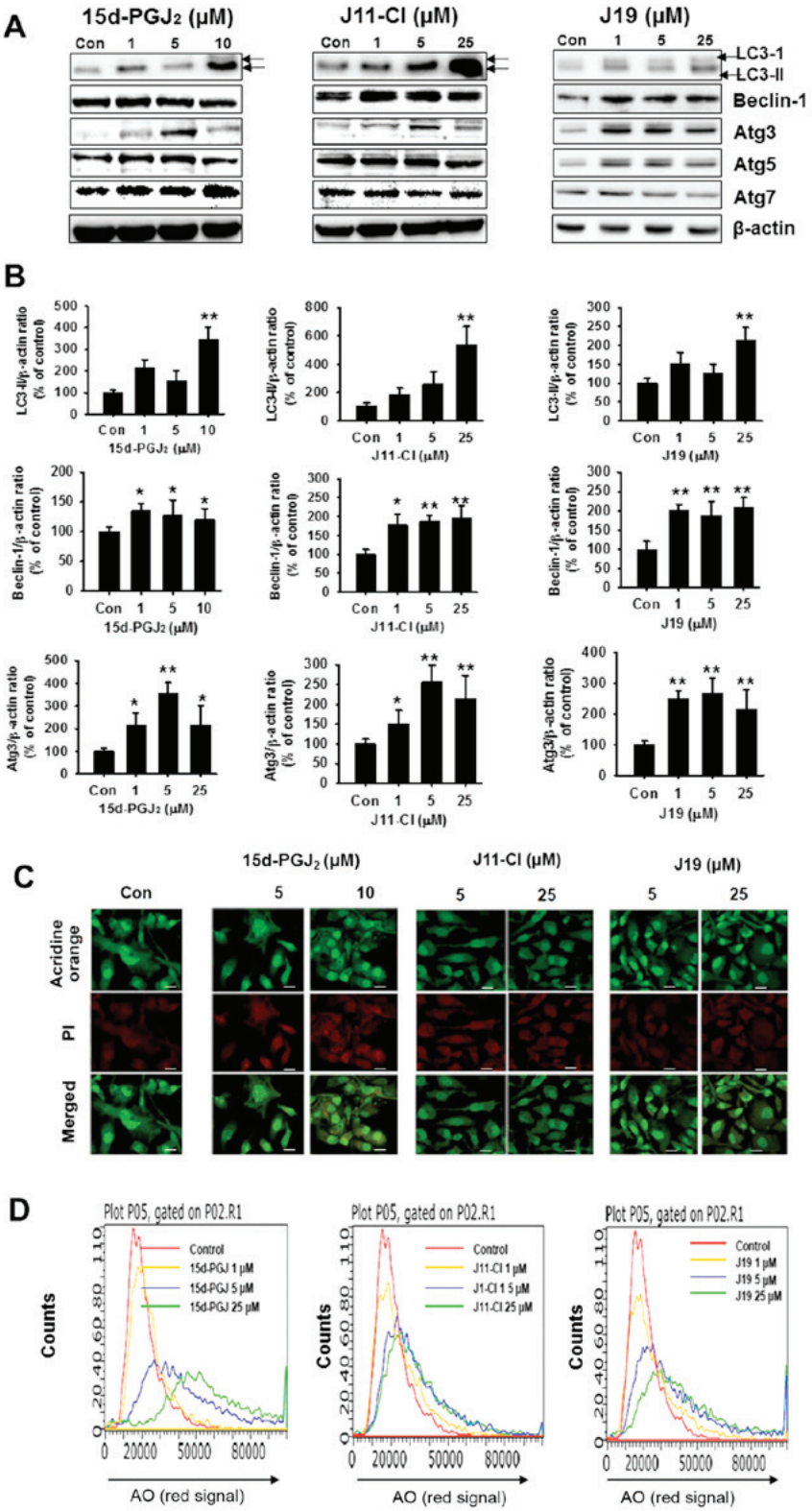

Figure 7. Effects of 15d-PGJ$_2$, J11-Cl and J19 on the autophagic pathway in SKOV3 cells. (A) SKOV3 cells were treated with 15d-PGJ$_2$, J11-Cl and J19 for 48 h, and expression levels of LC3-II, beclin-1, Atg3, Atg5 and Atg7 were determined using western blotting. (B) Quantification of western blot assays of three independent experiments using densitometry. *P<0.05, **P<0.01 vs. control. (C) Fluorescence of acridine orange-stained SKOV3 cells treated for 48 h with the indicated drug concentration using confocal microscopy. Scale bar, 50 μm. (D) Flow cytometric analysis following acridine orange staining and histogram profiles of control and drug-treated cells. 15d-PGJ$_2$, 15-deoxy-$\Delta^{12,14}$-prostaglandin J$_2$; LC3, light chain 3; Atg, autophagy-related; Con, control; AO, acridine orange.

that 3-MA alone was not cytotoxic to SKOV3 cells. However, the combination of 3-MA with 15d-PGJ$_2$, J19 or J11-C1 decreased cell death compared with individual treatment with 15d-PGJ$_2$, J19 or J11-C1 (Fig. 8A). To confirm the molecular mechanism and whether autophagic cell death was affected by 3-MA treatment, the expression levels of LC3, beclin-1,

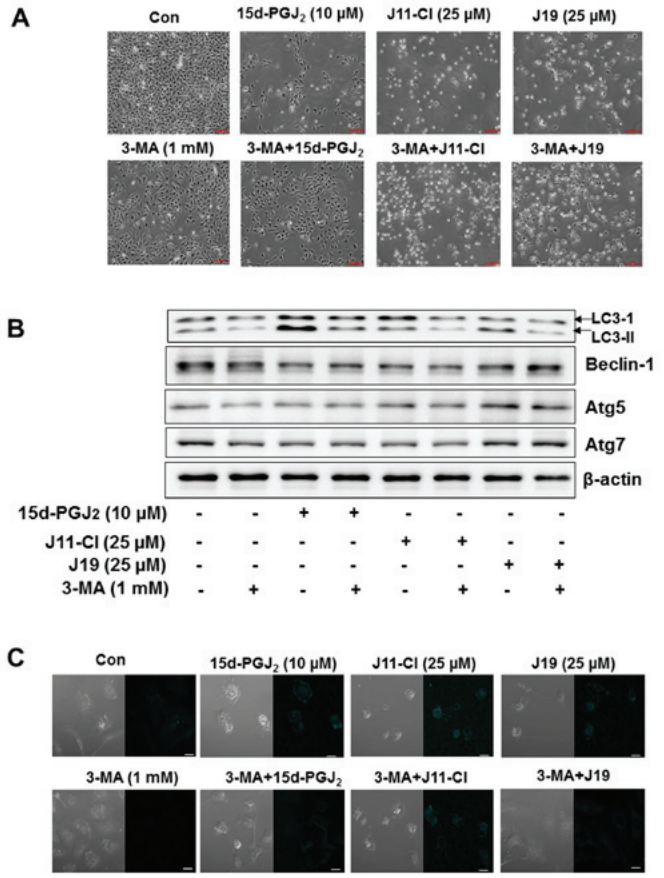

Figure 8. Effects of 3-MA on 15d-PGJ_2-, J11-Cl- and J19-induced autophagic death of SKOV3 cells. SKOV3 cells were cultured for 24 h in DMEM and exposed to 15d-PGJ_2, J11-Cl and J19 in the presence or absence of 3-MA (1 mM) for 48 h. Autophagy activity was assayed by MDC incorporation and western blot analysis with anti-LC3, anti-beclin-1, anti-Atg5 and anti-Atg7 antibodies. (A) Morphological changes in SKOV3 cells were determined by co-treatment with 3-MA (1 mM) and drugs. (B) Expression levels of LC3-II, beclin-1, Atg5 and Atg7 were determined using western blot analysis. β-actin was used as the internal control. (C) MDC staining indicated inhibition of autophagy in SKOV3 cells following co-treatment with 3-MA (1 mM) and drugs. Cells were examined using confocal microscopy. Scale bar, 10 μm. 3-MA, 3-methyladenine; 15d-PGJ_2, 15-deoxy-$\Delta^{12,14}$-prostaglandin J_2; LC3, light chain 3; Con, control; Atg, autophagy-related.

Atg5 and Atg7 were determined using western blotting. The expression levels of LC3-II and beclin-1 in 15d-PGJ_2-, J19-, or J11-C1 and 3-MA-treated SKOV3 cells were markedly decreased in SKOV3 cells (Fig. 8B). Next, the induction of autophagy was confirmed using MDC staining. The vital dye, which is commonly used to study autophagy, accumulates in autophagic vacuoles following a combination of ion trapping and specific interactions with vacuole membrane lipids (26,27). As presented in Fig. 8C, the autophagic cell death induced by 15d-PGJ_2 and its derivatives was decreased by co-treatment of SKOV3 cells with 3-MA.

Discussion

SIRT1 is the most widely studied member of the SIRT family and is known to modulate cell proliferation, differentiation, apoptosis, migration and invasion (3,7,28). SIRT1 controls cellular senescence and is overexpressed in specific cancer cell types (29,30). In the present study, the effect of 15d-PGJ_2 and its derivatives on SIRT1-mediated cell death pathways were investigated in SKOV3 cells. First, in the comparison of the cytotoxicity of the tested drugs, 15d-PGJ_2 exhibited more potent cytotoxicity compared with that of J11-Cl and J19, and decreased the expression levels of SIRT1 protein. Considering the reported electrophilic carbon atom (C9) of 15d-PGJ_2, we hypothesized that the inhibitory activity of 15d-PGJ_2 may be a consequence of the reactive carbon. The observation that 15d-PGJ_2 inhibited the gene expression of SIRT1 led to the consideration of whether 15d-PGJ_2 was able to directly inhibit the activity of SIRT1. To address this question, an acetylated p53 protein was selected as a substrate to determine SIRT1 activity. As expected, SIRT1/2 activity was significantly decreased by 15d-PGJ_2. To investigate the contribution of the C9 electrophilic carbon atom to this direct inhibitory activity, the molecular mechanics of 15d-PGJ_2, J11-Cl and J19 on SIRT1 were elucidated using docking simulations. Although the docking conformation of 15d-PGJ_2 with the SIRT1 protein did not reveal any nucleophile that reacted with C9 within 3 Å of the chemical, it revealed a higher binding affinity (best docking score, -9.43) compared with that of the other drugs, with the formation of three hydrogen bonds with Asp^{348} and Ile^{347}. The prior arrangement of the three hydrogen bonds also appeared to produce greater van der Waals interactions and electrostatic attractions for this drug. J11-Cl and J19 exhibited moderate (up to -7.34) and low docking scores (up to -4.33), respectively, to form two hydrogen bonds with Ile^{347} and Pro^{217} and a hydrogen bond with Arg^{274}; these configurations were less stable and potent compared with that of 15d-PGJ_2. Therefore, the strongly overlapping conformations of the tested drugs may explain the difference in binding affinity.

Next, to determine the mechanisms underlying the action of 15d-PGJ_2 and its derivatives, their effects on apoptotic and autophagic cell death pathways were investigated. First, cell cycle analysis was performed and it was identified that 15d-PGJ_2 and J19 significantly induced G_2/M phase arrest in SKOV3 cells. Previous studies indicated that sirtinol, a class III HDAC inhibitor, induced senescent-like growth arrest in breast cancer cells (31). SIRT1 has a more prominent function in controlling cell growth and survival as it exists in the same intracellular compartment as most cell cycle and cell death regulators (7,32). As expected, 15d-PGJ_2 and J19 treatment significantly increased cell cycle arrest in SKOV3 cells. These results are similar to those of a previous study, which indicated that the inhibition of SIRT1 activates p53 and Bax gene expression, thereby inducing cell cycle arrest and apoptosis (33). To investigate the mechanism underlying the anticancer effects of 15d-PGJ_2 and its derivatives, apoptotic cell death was assessed. Flow cytometric analysis revealed that 15d-PGJ_2 and J11-Cl markedly induced apoptosis and subsequently increased the sub-G_1 phase cell population. The downstream mechanism of apoptotic cell death was investigated. 15d-PGJ_2 and its derivatives increased the expression of Bax and decreased that of Bcl-2 in SKOV3 cells.

Autophagy, another cell death pathway that is important in tumor biology, was also investigated in SKOV3 cells following treatment with 15d-PGJ_2 and its derivatives. The inhibition of autophagy was suggested to allow the continued growth of pre-cancerous cells and autophagy may act as a tumor suppressor (34,35). Generally, cancer cells require

autophagy to survive nutrient-limiting and low-oxygen conditions, particularly in the poorly vascularized internal region of the tumor. According to the results of the present study, the autophagic process led to SKOV3 cell death following treatment with 15d-PGJ$_2$ or its derivatives. Significant increases in LC3B and Atg7 levels were observed following 15d-PGJ$_2$, J11-Cl and J19 treatment relative to the control cells, and these changes were markedly associated with the cytotoxic effects of these drugs. These results were confirmed by the induction of AVOs in the cytoplasm that was stained with acridine orange. Most importantly, novel mechanisms of action of 15d-PGJ$_2$ and its derivatives were revealed as the inhibition of SIRT1 regulated multiple mechanisms of tumor cell biology in SKOV3 cells.

In conclusion, the anticancer effects of newly synthesized 15d-PGJ$_2$ derivatives were investigated and the underlying molecular mechanisms of these drugs were elucidated. On the basis of the structural similarity of 15d-PGJ$_2$, J11-Cl and J19 bind to and inhibit SIRT1 enzyme activity. This indicated that J11-Cl and J19 may exert anticancer activity by binding to SIRT1, to enhance apoptotic and autophagic cell death of ovarian cancer cells. However, limitations to the present study require attention. Although the results of the present study clearly indicated that SIRT1 inhibition exhibited potent anticancer activity in ovarian cancer cells, further investigation to confirm the corresponding effect using *in vivo* xenograft models is warranted.

Acknowledgements

Not applicable.

Funding

The present study was supported by the National Research Foundation of Korea funded by the Korean government (grant nos. 2016R1A2B2011071 and 2016R1A4A1011189).

Availability of data and materials

The datasets generated during the study are available from the corresponding author on reasonable request.

Authors' contributions

HSK and MHK conceived and designed the experiments. IHT, EYP, PD and JYS performed the experiments and statistical analysis. SS, MHK and SYL performed the docking study. JHJ helped to analyze and interpret the data, and critically revised the manuscript. SYL, MHK and HSK drafted the manuscript. All authors read and approved the final paper.

Ethics approval and consent to participate

Not applicable.

Patient consent for publication

Not applicable.

Competing interests

The authors declare that they have no competing interests.

References

1. Nguyen LT, Chen H, Pollock C and Saad S: SIRT1 reduction is associated with sex-specific dysregulation of renal lipid metabolism and stress responses in offspring by maternal high-fat diet. Sci Rep 7: 8982, 2017.
2. Chan SH, Hung CH, Shih JY, Chu PM, Cheng YH, Lin HC and Tsai KL: SIRT1 inhibition causes oxidative stress and inflammation in patients with coronary artery disease. Redox Biol 13: 301-309, 2017.
3. Wang J, Kim TH, Ahn MY, Lee J, Jung JH, Choi WS, Lee BM, Yoon KS, Yoon S and Kim HS: Sirtinol, a class III HDAC inhibitor, induces apoptotic and autophagic cell death in MCF-7 human breast cancer cells. Int J Oncol 41: 1101-1109, 2012.
4. Park EY, Woo Y, Kim SJ, Kim DH, Lee EK, De U, Kim KS, Lee J, Jung JH, Ha KT, *et al*: Anticancer effects of a new SIRT inhibitor, MHY2256, against human breast cancer MCF-7 cells via regulation of MDM2-p53 binding. Int J Biol Sci 12: 1555-1567, 2016.
5. Peck B, Chen CY, Ho KK, Di Fruscia P, Myatt SS, Coombes RC, Fuchter MJ, Hsiao CD and Lam EW: SIRT inhibitors induce cell death and p53 acetylation through targeting both SIRT1 and SIRT2. Mol Cancer Ther 9: 844-855, 2010.
6. Kim HB, Lee SH, Um JH, Oh WK, Kim DW, Kang CD and Kim SH: Sensitization of multidrug-resistant human cancer cells to Hsp90 inhibitors by down-regulation of SIRT1. Oncotarget 6: 36202-36218, 2015.
7. Kim TH, Kim HS, Kang YJ, Yoon S, Lee J, Choi WS, Jung JH and Kim HS: Psammaplin A induces Sirtuin 1-dependent autophagic cell death in doxorubicin-resistant MCF-7/adr human breast cancer cells and xenografts. Biochim Biophys Acta 1850: 401-410, 2015.
8. Chu F, Chou PM, Zheng X, Mirkin BL and Rebbaa A: Control of multidrug resistance gene mdr1 and cancer resistance to chemotherapy by the longevity gene sirt1. Cancer Res 65: 10183-10187, 2005.
9. Smith WL: Prostanoid biosynthesis and mechanisms of action. Am J Physiol 263: F181-F191, 1992.
10. Straus DS, Pascual G, Li M, Welch JS, Ricote M, Hsiang CH, Sengchanthalangsy LL, Ghosh G and Glass CK: 15-deoxy-delta 12,14-prostaglandin J2 inhibits multiple steps in the NF-kappa B signaling pathway. Proc Natl Acad Sci USA 97: 4844-4849, 2000.
11. Cho WH, Choi CH, Park JY, Kang SK and Kim YK: 15-deoxy-(Delta12,14)-prostaglandin J2 (15d-PGJ$_2$) induces cell death through caspase-independent mechanism in A172 human glioma cells. Neurochem Res 31: 1247-1254, 2006.
12. de Jong E, Winkel P, Poelstra K and Prakash J: Anticancer effects of 15d-prostaglandin-J$_2$ in wild-type and doxorubicin-resistant ovarian cancer cells: Novel actions on SIRT1 and HDAC. PLoS One 6: e25192, 2011.
13. Ahmad P, Rasool S, Gul A, Sheikh SA, Akram NA, Ashraf M, Kazi AM and Gucel S: Jasmonates: Multifunctional roles in stress tolerance. Front Plant Sci 7: 813, 2016.
14. Dang HT, Lee HJ, Yoo ES, Hong J, Bao B, Choi JS and Jung JH: New jasmonate analogues as potential anti-inflammatory agents. Bioorg Med Chem 16: 10228-10235, 2008.
15. Choo J, Lee Y, Yan XJ, Noh TH, Kim SJ, Son S, Pothoulakis C, Moon HR, Jung JH and Im E: A novel peroxisome proliferator-activated receptor (PPAR)γ agonist 2-hydroxyethyl 5-chloro-4,5-didehydrojasmonate exerts anti-inflammatory effects in colitis. J Biol Chem 290: 25609-25619, 2015.
16. LigPrep, version 2.5. Schrödinger, LLC, New York, 2011.
17. Tripathi SK, Muttineni R and Singh SK: Extra precision docking, free energy calculation and molecular dynamics simulation studies of CDK2 inhibitors. J Theor Biol 334: 87-100, 2013.
18. Friesner RA, Banks JL, Murphy RB, Halgren TA, Klicic JJ, Mainz DT, Repasky MP, Knoll EH, Shelley M, Perry JK, *et al*: Glide: A new approach for rapid, accurate docking and scoring. 1. Method and assessment of docking accuracy. J Med Chem 47: 1739-1749, 2004.
19. Friesner RA, Murphy RB, Repasky MP, Frye LL, Greenwood JR, Halgren TA, Sanschagrin PC and Mainz DT: Extra precision glide: Docking and scoring incorporating a model of hydrophobic enclosure for protein-ligand complexes. J Med Chem 49: 6177-6196, 2006.

20. Halgren TA, Murphy RB, Friesner RA, Beard HS, Frye LL, Pollard WT and Banks JL: Glide: A new approach for rapid, accurate docking and scoring. 2. Enrichment factors in database screening. J Med Chem 47: 1750-1759, 2004.
21. Jacobson MP, Pincus DL, Rapp CS, Day TJ, Honig B, Shaw DE and Friesner RA: A hierarchical approach to all-atom protein loop prediction. Proteins 55: 351-367, 2004.
22. Murugan S and Amaravadi RK: Methods for studying autophagy within the tumor microenvironment. Adv Exp Med Biol 899: 145-166, 2016.
23. Chalkiadaki A and Guarente L: The multifaceted functions of sirtuins in cancer. Nat Rev Cancer 15: 608-624, 2015.
24. Pierzyńska-Mach A, Janowski PA and Dobrucki JW: Evaluation of acridine orange, LysoTracker Red, and quinacrine as fluorescent probes for long-term tracking of acidic vesicles. Cytometry A 85: 729-737, 2014.
25. Shingu T, Fujiwara K, Bögler O, Akiyama Y, Moritake K, Shinojima N, Tamada Y, Yokoyama T and Kondo S: Inhibition of autophagy at a late stage enhances imatinib-induced cytotoxicity in human malignant glioma cells. Int J Cancer 124: 1060-1071, 2009.
26. Paglin S, Hollister T, Delohery T, Hackett N, McMahill M, Sphicas E, Domingo D and Yahalom J: A novel response of cancer cells to radiation involves autophagy and formation of acidic vesicles. Cancer Res 61: 439-444, 2001.
27. de Duve C, de Barsy T, Poole B, Trouet A, Tulkens P and Van Hoof F: Commentary. Lysosomotropic agents. Biochem Pharmacol 23: 2495-2531, 1974.
28. He S, He C, Yuan H, Xiong S, Xiao Z and Chen L: The SIRT 3 expression profile is associated with pathological and clinical outcomes in human breast cancer patients. Cell Physiol Biochem 34: 2061-2069, 2014.
29. Wang P, Lv C, Zhang T, Liu J, Yang J, Guan F and Hong T: FOXQ1 regulates senescence-associated inflammation via activation of SIRT1 expression. Cell Death Dis 8: e2946, 2017.
30. Chen J, Zhang B, Wong N, Lo AW, To KF, Chan AW, Ng MH, Ho CY, Cheng SH, Lai PB, *et al*: Sirtuin 1 is upregulated in a subset of hepatocellular carcinomas where it is essential for telomere maintenance and tumor cell growth. Cancer Res 71: 4138-4149, 2011.
31. Ota H, Tokunaga E, Chang K, Hikasa M, Iijima K, Eto M, Kozaki K, Akishita M, Ouchi Y and Kaneki M: Sirt1 inhibitor, Sirtinol, induces senescence-like growth arrest with attenuated Ras-MAPK signaling in human cancer cells. Oncogene 25: 176-185, 2006.
32. Lin Z and Fang D: The roles of SIRT1 in cancer. Genes Cancer 4: 97-104, 2013.
33. Lee JT and Gu W: SIRT1: Regulator of p53 deacetylation. Genes Cancer 4: 112-117, 2013.
34. Yang ZJ, Chee CE, Huang S and Sinicrope FA: The role of autophagy in cancer: Therapeutic implications. Mol Cancer Ther 10: 1533-1541, 2011.
35. Sever ON and Demir OG: Autophagy: Cell death or survive mechanism. J Oncol Sci 3: 37-44, 2017.